Chemical Engineering Journal 168 (2011) 60–67

Contents lists available at ScienceDirect

Chemical Engineering Journal

journal homepage: www.elsevier.com/locate/cej

CFD simulation of water removal from water/ethylene glycol mixtures by pervaporation

Mashallah Rezakazemi, Mahnaz Shahverdi, Saeed Shirazian, Toraj Mohammadi*, Afshin Pak

Research Centre for Membrane Separation Processes, Faculty of Chemical Engineering, Iran University of Science and Technology (IUST), Narmak, Tehran, Iran

ARTICLE INFO

Article history:
Received 5 October 2010
Received in revised form 4 December 2010
Accepted 12 December 2010

Keywords:
Pervaporation
Numerical simulation
CFD
PVA membrane
Ethylene glycol

ABSTRACT

Pervaporation (PV) is a membrane technology that utilizes a non-porous membrane for the separation of liquid mixtures. PV using dense membranes has emerged as a promising new method for water removal from aqueous solutions. The mathematical model commonly used to predict the performance of PV is the resistance-in-series model. In the present study, a comprehensive mathematical model was developed to study the performance of PV. The model is based on solving the conservation equations for water in the membrane module. The conservation equations including continuity and momentum equations were derived and solved numerically using finite element method (FEM). Computational fluid dynamics (CFD) technique was applied to solve the model equations. The model was then validated using the experimental data obtained from PV experiments with poly(vinyl alcohol) (PVA) membrane. The simulation results were in good agreement with the experimental data for different values of feed flow rates and temperatures. The modeling findings also indicated that permeate flux increases with increasing feed flow rate and temperature in the membrane module. The simulation results revealed that the developed model can provide a general simulation of transport in PV.

1. Introduction

Ethylene glycol (EG) is an important chemical material which is mostly used as nonvolatile antifreeze and coolant as well as an intermediate in manufacture of polyesters. EG is commercially produced using direct oxidation of ethylene to ethylene oxide followed by hydrolysis of ethylene oxide in which, excess water is added to ethylene oxide to increase EG content and decrease diethylene glycol (DEG) and triethylene glycol (TEG) contents [1]. The maximum amount of EG is achieved when the mole ratio of water to ethylene oxide is about 22:1. In this case EG contains about 86 wt.% water [2]. The excess water should be removed from the hydrolysis medium.

Pervaporation (PV) technology compared with distillation process has been found a better choice for liquid separation with close boiling point, azeotropic or isomeric mixtures [3]. Currently, industrial applications of PV technology are divided into three categories: (i) dehydration of alcohols, (ii) dehydration of organic solvents using hydrophilic or charged polymeric membranes and (iii) removal of small quantities of volatile organic compounds from water using hydrophobic membranes [4]. The previous work proved that PV using poly(vinyl alcohol) (PVA) dense membrane has a good performance for dehydration of EG/water liquid mixture [5].

The mass transfer through porous and non-porous membranes has been studied extensively. Many models have been proposed to predict mass transfer flux, such as solution-diffusion model, Maxwell–Stefan theory, pore flow model, and resistance-in-series model. Among them, solution-diffusion model is most widely used in describing PV transport. Considerable attention should be focused on the mass transfer behavior because of its vital role for optimizing PV process [6–9]. There are two approaches for modeling of mass transfer in PV. The first one is based on resistance-in-series model. In this model, the resistances in the liquid phase boundary layer and the membrane phase are considered in series, while the resistance at the permeate side is neglected because of high vacuum applied [10]. The latter modeling approach needs mass transfer coefficients for liquid and membrane phases to be estimated. The experimental correlations are extensively used to estimate mass transfer coefficients that are dependent on Reynolds and Schmidt numbers. Calculation of mass transfer coefficients by this method should be validated using experiments. A mathematical model containing mass transfer under non-isothermal conditions was developed with strong contribution of polarization concentration by Gómez et al. [11] to describe the behavior of a plate-and-frame PV membrane module. Simulation results showed temperature and flow rate significantly influence the liquid mass transport coefficient. Recently, based on

* Corresponding author. Tel.: +98 21 789 6621; fax: +98 21 789 6620.
E-mail address: torajmohammadi@iust.ac.ir (T. Mohammadi).

1385-8947/$ – see front matter © 2010 Elsevier B.V. All rights reserved.
doi:10.1016/j.cej.2010.12.034

Nomenclature

EG	ethylene glycol
DEG	diethylene glycol
TEG	triethylene glycol
PVA	poly(vinyl alcohol)
CFD	computational fluid dynamics
FEM	finite element method
PV	pervaporation
j	total flux (kg/m^2 h)
M	permeate weight (kg)
A	effective membrane surface area (m^2)
t	pervaporation time (h)
R	reaction term (mol/m^3 s)
C	concentration of water (mol/m^3)
D	diffusion coefficient (m^2/s)
V	velocity vector (m/s)
η	dynamic viscosity (kg/m s)
ρ	density of the fluid (kg/m^3)
P	pressure (Pa)
F	body force term (N)
x	x coordinate (m)
y	y coordinate (m)

Subscripts

w	water
y	y-direction
m	membrane
i	interface

multi-fields synergy theory, a mass transfer model for the separation of binary mixture in PV process was presented. The mechanism of sorption–diffusion–desorption was applied in this model. The model related diffusion coefficient to feed concentration and temperature. To validate the model with experimental data, Lei et al. [12] prepared a PV cell to separate tert-butyl alcohol/water mixture. From experimental and simulation results, good agreement was achieved.

The second approach is based on the solving conservation equations for penetrants in the liquid and membrane phases. In this approach, conservation equations including continuity, energy and momentum equations are derived and solved simultaneously by appropriate numerical method based on computational fluid dynamics (CFD) techniques. The applications of CFD are usually carried out in three steps: preprocessing, processing, and post processing, respectively. Villaluenga and Cohen [13] developed a numerical model of non-isothermal to investigate velocity, concentration and temperature fields in a rectangular PV membrane module geometry. Their modeling findings showed that the nonlinear character of concentration and temperature boundary-layers are most significant near the membrane surface.

Liu et al. [14] applied the CFD technique to obtain velocity and concentration distributions in liquid boundary layer of a slit membrane channel. They modeled concentration polarization in a PV membrane module. CFD was found to be useful for the simulation of pervaporative mass transfer in various membrane modules. Liu et al. [15] also provided a CFD modeling and simulation framework to describe the effect of baffle on mass transfer in a slit-type PV module. The module consisted of mixing-promoting baffles to remove volatile organic compounds significantly and improve mass transfer. Simulation results showed improvements of the average mass transfer coefficient with increasing the baffle height of the slit within the flow channel as compared with the module with no baffle. Simulation results also indicated a good agreement with the experimental results, Reynolds number must be below 1000.

As understood, there is a definite need for a comprehensive model which can provide a general simulation of separation process in PV. The main objective of the present study is to develop and solve a two dimensional mass transfer model for the simulation of water removal from EG/water mixtures by PV process. Simulations are based on solving the conservation equations including mass and momentum transfer for water in the feed and the membrane phases. The developed model is capable of predicting mass transport in the feed and the membrane sides. It also considers axial diffusion in the feed phase. The simulation results are then validated with the experimental data obtained from our previous work on separation of EG/water mixtures by PV through a novel PVA/polypropylene composite membrane [5].

2. Experimental

PVA/PP composite membranes were prepared using phase inversion method and used in PV experiments for the removal of water from EG/water liquid mixtures. The detailed procedure of membrane preparation was described elsewhere [5].

Feed solutions, EG/water mixture containing 10 wt.% water were prepared. Temperature was adjusted at 60, 70 and 80 °C; meanwhile, recirculation flow rate velocity was kept constant at 1–2 L/min using a bypass pump to achieve a Reynolds number between 100 and 150.

PVA membrane employed in this study had a thickness of 7 μm. All experiments in this study were performed using the same membrane. PV experiments were carried out using an apparatus as shown in Fig. 1. The membrane was housed in a PV cell that consisted of two detachable stainless-steel parts. The membrane had an effective area of approximately 0.00104 m^2. Rubber O-rings were used to provide a pressure tight seal between the membrane and the PV cell. Physical dimensions, length and diameter, of PV cell were 0.13 m and 0.06 m, respectively. Fig. 2 indicates the module dimensions.

A pump was employed to recirculate feed solution. Feed temperature was controlled within 3 °C using a thermostat. Volume of feed tank was 7 L which was very big compared with permeation volume; therefore, variation of feed concentration during a period of 1 h was negligible. In all experiments, feed was kept at atmospheric pressure, whereas permeate pressure was maintained in a range of 8–10 mbar by an oil sealed vacuum pump (MOTO GEN 80-4B with RPM 1380, Iran). Permeate samples were condensed and collected in a Pyrex glass condenser kept inside a cryogenic trap at −35 °C. An accurate refractometer (DR-A1) was employed to analyze alcohol concentration in permeate samples. Some samples were also analyzed using a Varian gas chromatography (model STAR 3400 CX) equipped with a flame ionization detector for confirmation. Permeate flux was calculated using the following equation:

$$j = \frac{M}{At} \quad (1)$$

where j is the total flux (kg/m^2 h), M is the permeate weight (kg), A is the effective membrane surface area (m^2) and t is the PV time (h).

3. Model development

Fig. 3 shows the model domain used for modeling. The feed involving a mixture of 10 wt.% water and 90 wt.% ethylene glycol (EG) flows through the upper side of the membrane module ($y = 0$). The feed exits from the upper side of the feed compartment and recirculates inside the module. The membrane at $y = L$ (membrane length) is closed.

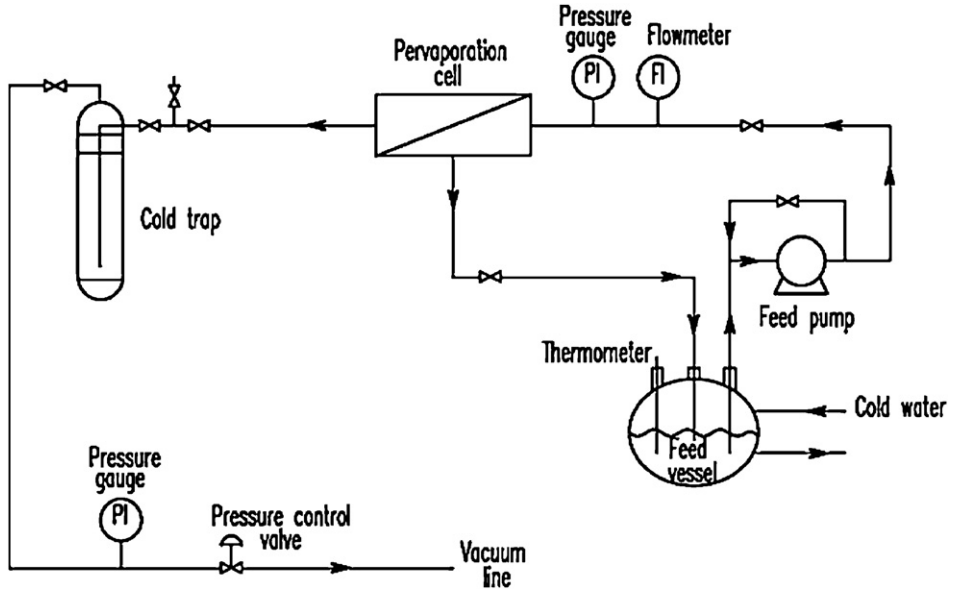

Fig. 1. Schematic diagram of experimental setup for PV.

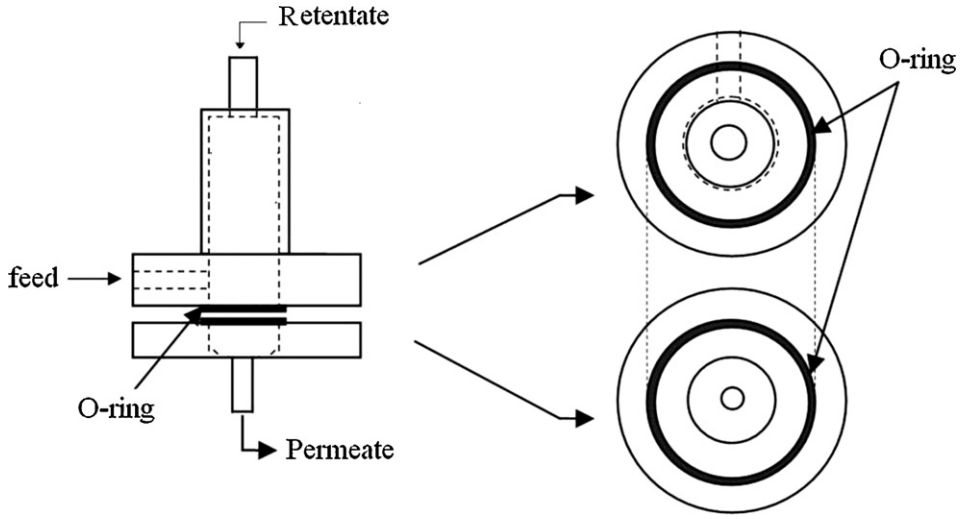

Fig. 2. Schematic diagram of experimental module for PV.

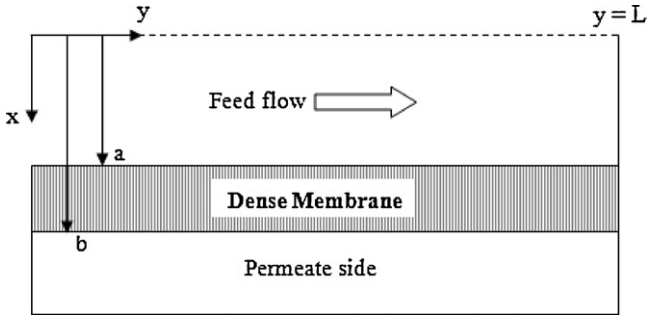

Fig. 3. Model domain.

The mathematical model is built considering the following assumptions:

(1) Steady state and isothermal conditions.
(2) Laminar flow for the feed in the membrane module.
(3) Thermodynamic equilibrium at the feed–membrane interface.
(4) Only water penetrates through the membrane.
(5) Mass transfer resistance of support layer is assumed to be negligible.

The main equation that describes the transfer of water from the feed phase to the permeate side is continuity equation. This equation is derived from mass balance of water within an element. The differential form of continuity equation for water may be written as [16]:

$$\frac{\partial C_w}{\partial t} + \nabla \cdot (-D_w \nabla C_w + C_w V) = R_w \quad (2)$$

where C_w denotes the concentration of water (mol/m^3), D_w denotes its diffusion coefficient (m^2/s), V denotes the velocity vector (m/s) and R_w denotes the reaction term (mol/m^3 s). The velocity vector can be expressed analytically or obtained by coupling a momentum balance to the equation system. This equation is also called convection and diffusion equation.

Eq. (2) is the main equation of mass transfer. This equation should be solved numerically to obtain the concentration distri-

bution of water in the membrane module. To solve the continuity equation (Eq. (2)), velocity distribution is needed. Velocity distribution is obtained by solving the momentum equation, i.e. Navier–Stokes equations. Therefore, the momentum and continuity equations should be coupled and solved simultaneously to obtain the concentration distribution of water. The Navier–Stokes equations describe flow in viscous fluids through momentum balances for each of the components of the momentum vector in all spatial dimensions [16]:

3.1. Feed phase equations

The steady state continuity equation for transport of water in the feed phase is obtained using Fick's law of diffusion for estimation of diffusive flux:

$$D_w \left[\frac{\partial^2 C_{\text{w-feed}}}{\partial x^2} + \frac{\partial^2 C_{\text{w-feed}}}{\partial y^2} \right] = V_y \frac{\partial C_{\text{w-feed}}}{\partial y} \tag{3}$$

In laminar flow, Navier–Stokes equations can be applied as:

$$\begin{aligned} &-\nabla \cdot \eta(\nabla V_y + (\nabla V_y)^T) + \rho(V_y \cdot \nabla)V_y + \nabla p = F \\ &\nabla \cdot V_y = 0 \end{aligned} \tag{4}$$

where η denotes the dynamic viscosity (kg/m s), V_y denotes the velocity vector in y direction (m/s), ρ denotes the density of the fluid (kg/m^3), P denotes the pressure (Pa) and F denotes a body force term (N). The feed flows in the y-direction of the membrane module, therefore y-velocity should be solved.

The boundary conditions for the continuity equation are:

$$\text{at } y = 0, \quad C_{\text{w-feed}} = C_0 \quad \text{(inlet concentration)} \tag{5}$$

$$\text{at } y = L, \quad \frac{\partial C_{\text{w-feed}}}{\partial y} = 0 \quad \text{(insulation boundary)} \tag{6}$$

$$\text{at } x = 0, \quad \text{convective flux} \tag{7}$$

The convective flux boundary condition assumes that all mass passing through this boundary is convection-dominated. This firstly assumes that any mass flux due to diffusion across this boundary is zero.

$$\text{at } x = a, \quad C_{\text{w-feed}} = C_{\text{w-feed}/m} \quad \text{(insulation boundary)} \tag{8}$$

where m is partition coefficient for water between the feed and the membrane.

The boundary conditions for Navier–Stokes equations are:

$$\text{at } y = 0, \quad V_y = V_0 \quad \text{(inlet velocity)} \tag{9}$$

$$\text{at } y = L, \quad V = 0 \quad \text{(no slip condition)} \tag{10}$$

$$\text{at } x = 0, \quad p = p_{\text{atm}} \tag{11}$$

$$\text{at } x = a, \quad V = 0 \quad \text{(no slip condition)} \tag{12}$$

3.2. Membrane equations

The steady state continuity equation for transport of water through the membrane is as follows:

$$D_{\text{w-membrane}} \left[\frac{\partial^2 C_{\text{w-membrane}}}{\partial x^2} + \frac{\partial^2 C_{\text{w-membrane}}}{\partial y^2} \right] = 0 \tag{13}$$

The boundary conditions for the continuity equation in the membrane are:

$$\text{at } x = a, \quad C_{\text{w-membrane}} = C_{\text{w-feed}} \times m$$

$$\text{at } x = b, \quad C_{\text{w-membrane}} = 0 \quad \text{(vacuum)} \tag{14}$$

Fig. 4. Magnified segments of the mesh used in the numerical simulation. There are 3904 elements in total for the whole domain.

$$\text{at } y = 0 \text{ and } y = L, \quad \frac{\partial C_{\text{w-membrane}}}{\partial y} = 0$$
$$\text{(insulation boundary)} \tag{15}$$

Temperature dependence of diffusion and partition coefficients can be approximated as [17–20]:

$$D_{\text{m,i}} = D^0_{\text{m,i}} \exp\left(-\frac{E_{\text{D}}}{RT}\right) \tag{16}$$

$$H_{\text{m,i}} = H^0_{\text{m,i}} \exp\left(-\frac{\Delta H_{\text{s}}}{RT}\right) \tag{17}$$

where ΔH_{s} and E_{D} are the enthalpy of solution of component i in the membrane and the diffusion activation energy, respectively, and $D^0_{\text{m,i}}$ and $H^0_{\text{m,i}}$ are the corresponding pre-exponential factors.

3.3. Numerical solution of model equations

The derived conservation equations including concentration and momentum equations related to the feed and the membrane with the appropriate boundary conditions were solved numerically using COMSOL Multiphysics software version 3.2. This software employs finite element method (FEM) for numerical solutions of model equations. The use of FEM method allows mass conservation in the domain; therefore "numerical loss" of mass in the computational domain is not a major concern. The applicability, validity and robustness of the FEM method for the kind of domain encountered in the present work were demonstrated by a number of previous authors [21–27]. The FEM was combined with adaptive meshing and error control using numerical solver of UMFPACK. This solver is an implicit time-stepping scheme, which is well suited for solving stiff and non-stiff non-linear boundary value problems [21]. An IBM-PC-Pentium 5 (CPU speed was 2600 MHz and 2 GB of RAM) was used to solve the set of equations. The computational time for solving the set of equations was about 2 min. It should be pointed out that the COMSOL mesh generator creates triangular meshes that are isotropic in size. A large number of elements were then created with scaling. A scaling factor was employed in y direction due to large difference between y and x dimensions. COMSOL automatically scaled back the geometry after meshing. This generated an anisotropic mesh with 3904 elements. Adaptive mesh refinement in COMSOL, which generates the best and minimal meshes, was used to mesh the module geometry. Fig. 4 indicates the meshes generated by COMSOL software.

4. Results and discussion

4.1. Model validation

In order to verify the mass transfer model used for simulation, the simulation results were compared with the experimental

Table 1
Comparison between experimental and simulated values for the PV flux of water.

Temperature (°C)	Water concentration in permeate (wt.%)	Feed flow rate (L/min)	Permeate flux of water (kg/m^2 h)		Error (%)
			Experimental	Simulation	
60	0.995	1.0	0.1058	0.1133	7.07
	0.995	1.5	0.6041	0.6302	4.30
	0.991	2.0	1.0844	1.2051	11.12
70	0.990	1.0	0.2182	0.2462	12.80
	0.989	1.5	0.6560	0.6802	3.68
	0.969	2.0	0.9555	0.9937	3.99
80	0.988	1.0	0.6331	0.6653	5.08
	0.987	1.5	1.0240	1.1380	11.13
	0.939	2.0	0.9521	0.9874	3.71

values. The experimental results were for PV of a water/EG mixture using a dense PVA membrane. In this section, the PV flux of water calculated by simulation is compared with the experimental values to verify the simulation results. Table 1 shows the comparison between experimental and simulated values for the PV flux of water.

As shown in Table 1, the simulation results match well with the experimental data. As observed, the calculated permeate fluxes are always more than the experimental data. This is because that the feed composition was assumed constant. However, in the experiments, water concentration in the feed varied during the experiments because of recirculating the feed phase. Assuming constant feed concentration, calculated the permeate flux more than the experimental value because of higher concentration difference.

Temperature ranged from 60 to 80 °C in the experiments. As observed in Table 1, total permeate flux increases with increasing temperature. At high feed flow rate and temperature, swelling happens and EG penetrates through the membrane and reduces the water concentration at the permeate side. The developed model cannot predict the swelling phenomenon.

With increasing temperature, diffusivity of water in the feed and the membrane phase increases whereas the partition coefficient (m) for water between the feed phase and the membrane decreases. Therefore, there are two parameters acting opposite of each other. Diffusivity is the predominant parameter and there is an enhancement of permeate flux with increasing temperature (Table 1).

4.2. Concentration distribution of water

Fig. 5 represents the dimensionless concentration distribution (C/C_0) of water in the feed and the membrane within the module. The feed mixture containing water/EG flows from one side of the module ($y = 0$) where the concentration of water is the highest (C_0). As the feed flows through the feed side, water is transferred to the membrane due to the concentration difference (driving force). The mechanism of mass transfer in the feed side of the module is convection and diffusion. The mass (water) is transferred through the dense membrane via diffusion mechanism. Water after passing through the membrane which is transferred only by diffusion mechanism then is evaporated by the induced vacuum in the permeate side. The concentration of water at the permeate–membrane interface is assumed to be zero because of low pressure.

Fig. 6 illustrates the axial concentration distribution of water in the feed side along the membrane module at different feed flow rates. As shown, increasing feed flow rate increases the water content at the feed compartment which in turn increases the driving force for the mass transfer from the feed to the membrane and the permeates. Increasing driving force increases the permeate water flux in the membrane module.

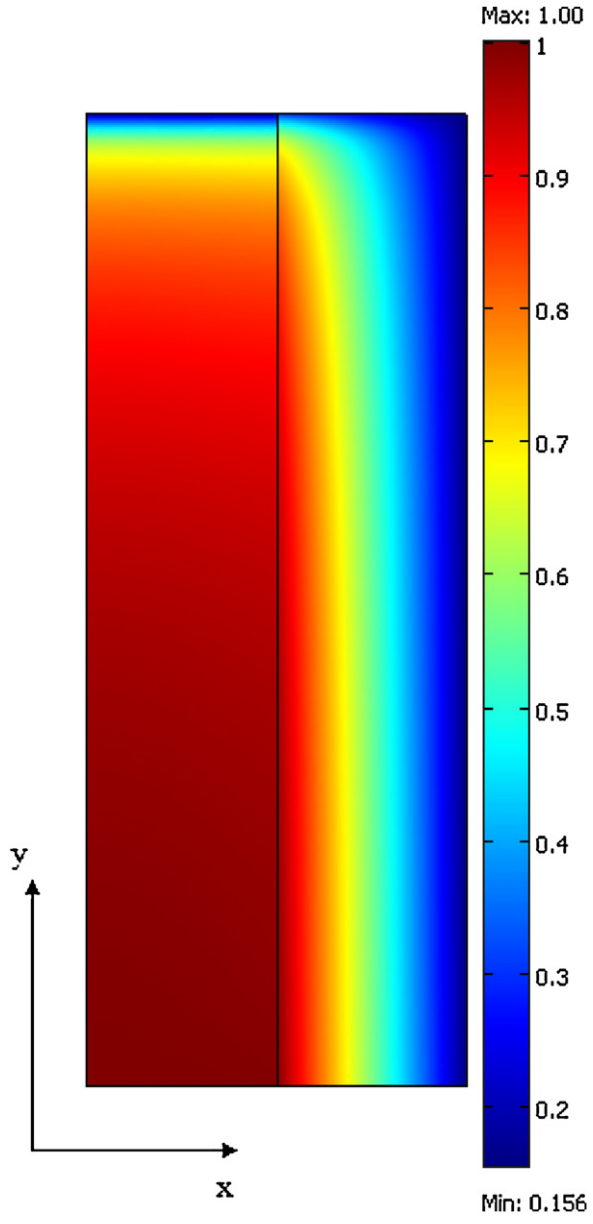

Fig. 5. A representation of the concentration distribution of water (C_w/C_0) in the membrane module. Feed flow rate = 1 L/min; water inlet concentration = 10 wt.%; temperature = 60 °C.

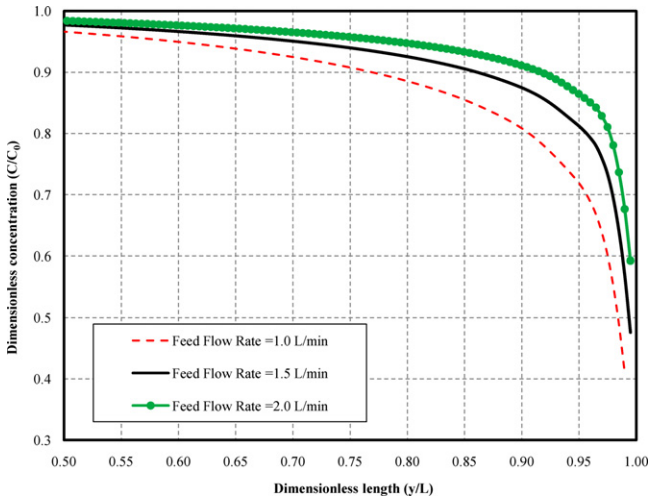

Fig. 6. Axial concentration distribution of water (C_w/C_0) along the membrane module at different feed flow rates; water inlet concentration = 10 wt.%; temperature = 60 °C.

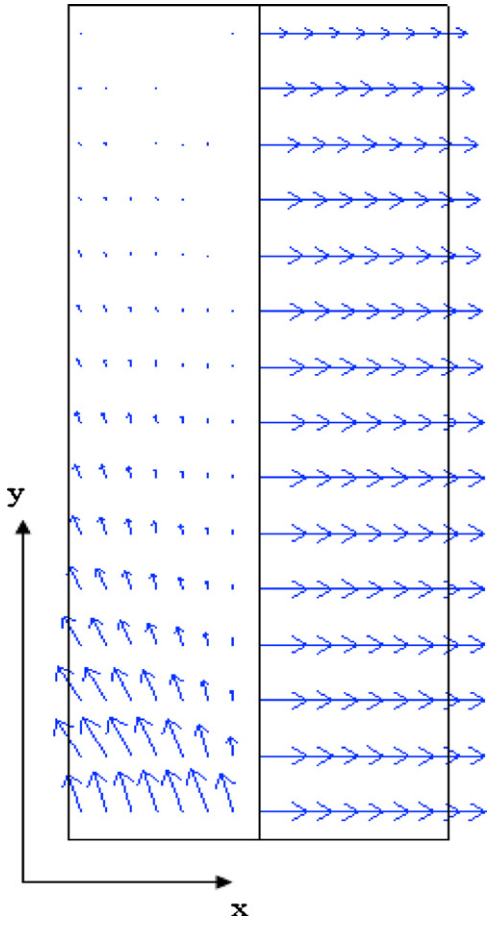

Fig. 7. The permeate water flux distribution in the module. Feed flow rate = 1 L/min, inlet concentration of water = 10 wt.%; temperature = 60 °C. The two domains from left to right are the feed channel and the membrane, respectively.

4.3. Permeate flux distribution of water

Fig. 7 illustrates the permeate water flux in the membrane module. The permeate flux of water is constituted of two mass fluxes including diffusion and convection mass fluxes. In the feed channel, mass transfer mechanisms are diffusion and convection due to the concentration gradient of water and feed velocity. Therefore, permeate flux is in two directions (see Fig. 7). At the inlet of the feed side, the permeate water flux is the highest because of high concentration gradient of water. As feed flows along the module length, the driving force reduces and the permeate water flux decreases (see Fig. 7). The main equation that describes the transport through the membrane is Fick's law of diffusion which considers only diffusional mass transfer. The concentration gradient of water in the membrane is in x direction because of insulation boundaries at the top and the bottom of membrane and also low pressure at the permeate side ($x = b$). Hence, in the dense membrane, the permeate water flux is uniform and in x direction.

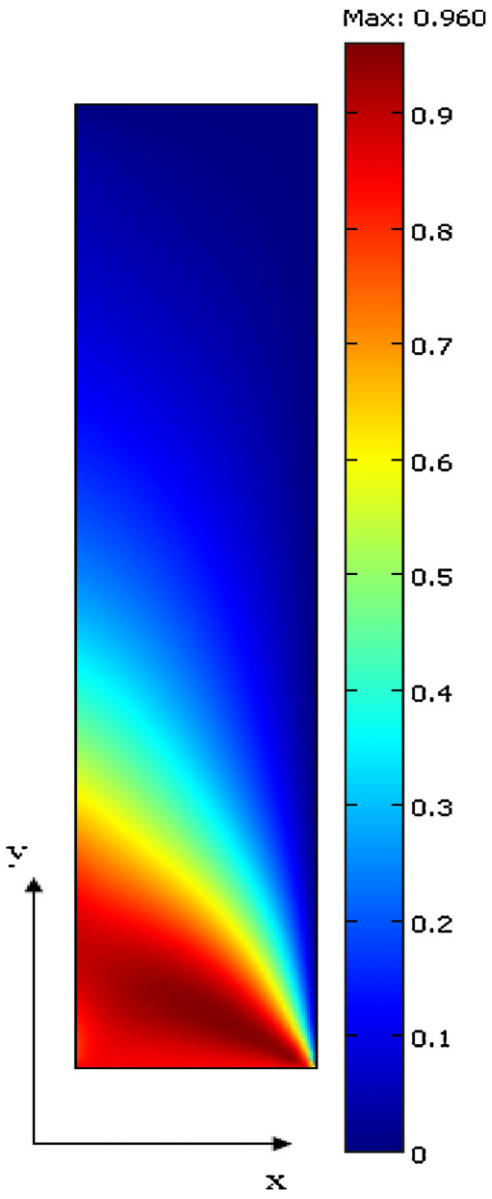

Fig. 8. Velocity field in the feed side of the module. Feed flow rate = 1 L/min, inlet concentration of water = 10 wt.%; temperature = 60 °C.

4.4. Velocity distribution field

The velocity in the feed side of the membrane module is illustrated in Fig. 8. The velocity profile in the feed side of the membrane module was simulated by solving the Navier–Stokes equations. The velocity profile along the membrane module is also shown

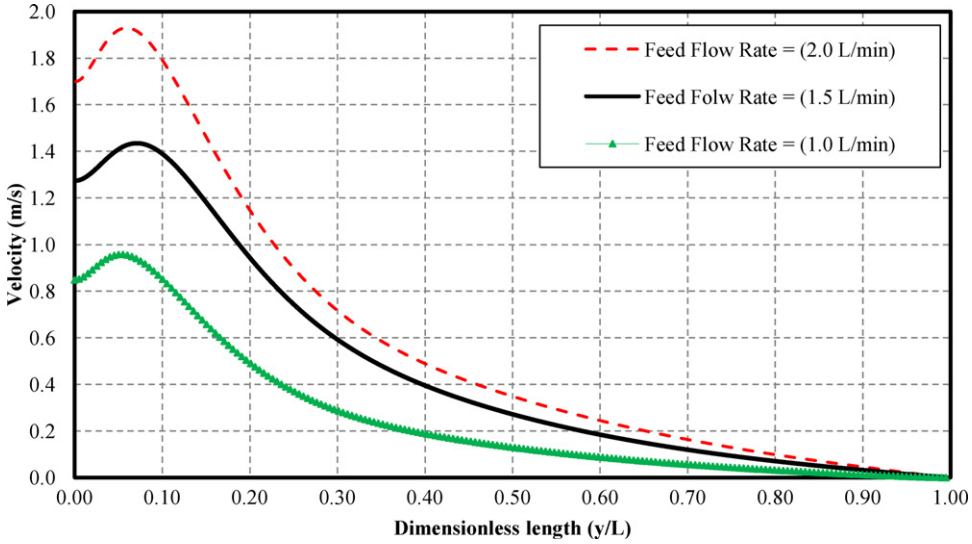

Fig. 9. Axial velocity profile along the feed side of module. Feed flow rate = 1 L/min, inlet concentration of water = 10 wt.%; temperature = 60 °C.

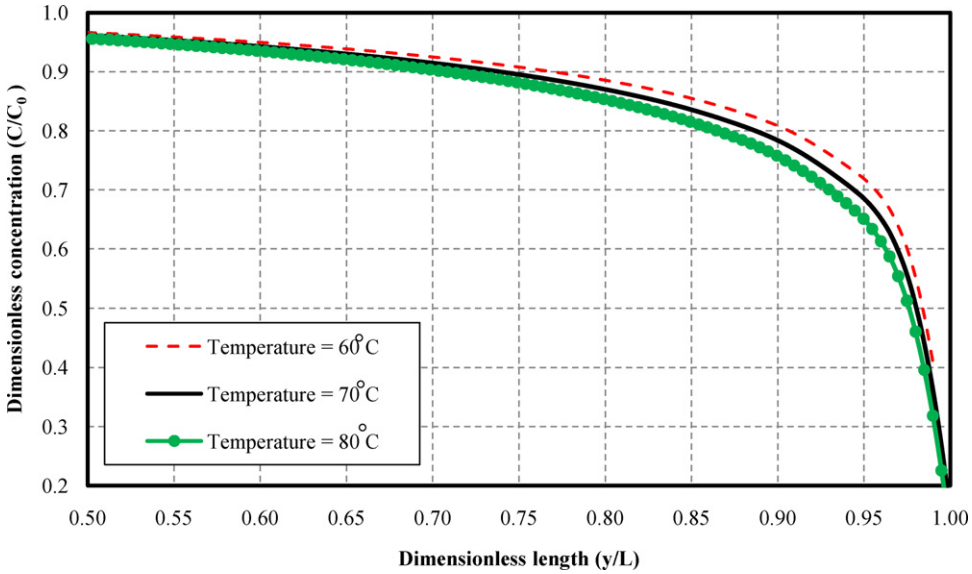

Fig. 10. Effect of temperature on concentration profile along the feed side of the module. Feed flow rate = 1 L/min, inlet concentration of water = 10 wt.%

in Fig. 9. In membrane module, the feed exits from the left side of the module. The two sides of the feed in the module are surrounded by solid phase ($x = a$; $y = L$). Fig. 9 indicates that there is a maximum velocity at a region near the entrance. The maximum velocity increases with increasing feed flow rate in the membrane module.

4.5. Effect of temperature

Effects of feed temperature on the permeate flux of water are illustrated in Fig. 10. As observed, increasing temperature causes the concentration of water decreases in the feed side. This means that the permeate flux of water increases with increasing temperature. This can be attributed to the fact that as temperature decreases, the solubility of water increases and the volumetric feed flow rate decreases, which gives combined favorable effects on the water removal. On the other hand, with decreasing temperature, liquid-phase diffusion coefficients decrease, giving unfavorable effect on the water removal. Since the unfavorable effect is more pronounced than the favorable effect, a net enhancement of water removal is observed with increasing temperature.

5. Conclusions

Removal of water from ethylene glycol (EG)/water liquid mixture by pervaporation (PV) was studied theoretically and experimentally in this work. A comprehensive 2-dimensional mathematical model was developed to predict the transport of water in PV. The model was based on solving the conservation equations for water in the membrane module. The conservation equations including continuity and momentum equations were derived and solved numerically for water. The model was then verified by the experimental data obtained from PV experiments using a synthesized poly(vinyl alcohol) (PVA) composite membrane. The comparisons between experimental and simulated permeate fluxes showed a good agreement for different values of feed flow rates and temperatures. Effects of various parameters on the permeate flux of water were investigated. The modeling findings also indicated

that the permeate flux increases with increasing feed flow rate and temperature in the membrane module.

References

[1] M.W. Forkner, J.H. Robson, W.M. Snellings, A.E. Martin, F.H. Murphy, T.E. Parsons, Encyclopedia of Chemical Technology, 4th ed., John Wiley & Sons, New York, 1994.
[2] O.G. Nik, A. Moheb, T. Mohammadi, Separation of ethylene glycol/water mixtures using NaA zeolite membranes, Chemical Engineering & Technology 29 (2006) 1340–1346.
[3] A.W. Verkerk, P. van Male, M.A.G. Vorstman, J.T.F. Keurentjes, Description of dehydration performance of amorphous silica pervaporation membranes, Journal of Membrane Science 193 (2001) 227–238.
[4] S.Q. Zhang, A.E. Fouda, T. Matsuura, A study of pervaporation of aqueous benzyl alcohol solution by polydimethylsiloxane membrane, Journal of Membrane Science 70 (1992) 249–255.
[5] M. Shahverdi, T. Mohammadi, A. Pak, Separation of ethylene glycol–water mixtures with composite poly(vinyl alcohol)–polypropylene membranes, Journal of Applied Polymer Science 119 (2011) 1704–1710.
[6] F. Peng, F. Pan, D. Li, Z. Jiang, Pervaporation properties of PDMS membranes for removal of benzene from aqueous solution: experimental and modeling, Chemical Engineering Journal 114 (2005) 123–129.
[7] S.V. Satyanarayana, A. Sharma, P.K. Bhattacharya, Composite membranes for hydrophobic pervaporation: study with the toluene–water system, Chemical Engineering Journal 102 (2004) 171–184.
[8] S. Tan, L. Li, Z. Zhang, Z. Wang, The influence of support layer structure on mass transfer in pervaporation of composite PDMS–PSF membranes, Chemical Engineering Journal 157 (2010) 304–310.
[9] A. Lovasz, P. Mizsey, Z. Fonyo, Methodology for parameter estimation of modelling of pervaporation in flowsheeting environment, Chemical Engineering Journal 133 (2007) 219–227.
[10] A.A. Ghoreyshi, M. Jahanshahi, K. Peyvandi, Modeling of volatile organic compounds removal from water by pervaporation process, Desalination 222 (2008) 410–418.
[11] P. Gómez, R. Aldaco, R. Ibáñez, I. Ortiz, Modeling of pervaporation processes controlled by concentration polarization, Computers & Chemical Engineering 31 (2007) 1326–1335.
[12] Z. Lei, Y. Wu, S. Lu, B. Yang, Mass transfer modeling in pervaporation based on multi-fields synergy theory, Chinese Journal of Chemical Engineering 16 (2008) 79–83.
[13] J.P.G. Villaluenga, Y. Cohen, Numerical model of non-isothermal pervaporation in a rectangular channel, Journal of Membrane Science 260 (2005) 119–130.
[14] S.X. Liu, M. Peng, L. Vane, CFD modeling of pervaporative mass transfer in the boundary layer, Chemical Engineering Science 59 (2004) 5853–5857.
[15] S.X. Liu, M. Peng, L.M. Vane, CFD simulation of effect of baffle on mass transfer in a slit-type pervaporation module, Journal of Membrane Science 265 (2005) 124–136.
[16] R.B. Bird, W.E. Stewart, E.N. Lightfoot, Transport Phenomena, 2nd ed., John Wiley & Sons, New York, 1960.
[17] Z. Yuzhong, Z. Keda, X. Jiping, Preferential sorption of modified PVA membrane in pervaporation, Journal of Membrane Science 80 (1993) 297–308.
[18] J.-W. Rhim, R.Y.M. Huang, Prediction of pervaporation separation characteristics for the ethanol–water–nylon-4 membrane system, Journal of Membrane Science 70 (1992) 105–118.
[19] C. Dotremont, B. Brabants, K. Geeroms, J. Mewis, C. Vandecasteele, Sorption and diffusion of chlorinated hydrocarbons in silicalite-filled PDMS membranes, Journal of Membrane Science 104 (1995) 109–117.
[20] R.Y.M. Huang, Pervaporation Membrane Separation Process, Elsevier, Amsterdam, The Netherlands, 1991.
[21] M.H. Al-Marzouqi, M.H. El-Naas, S.A.M. Marzouk, M.A. Al-Zarooni, N. Abdullatif, R. Faiz, Modeling of CO_2 absorption in membrane contactors, Separation and Purification Technology 59 (2008) 286–293.
[22] U. Shavit, G. Bar-Yosef, R. Rosenzweig, S. Assouline, Modified Brinkman equation for a free flow problem at the interface of porous surfaces: the Cantor-Taylor brush configuration case, Water Resources Research 38 (2002) 1320–1334.
[23] U. Shavit, R. Rosenzweig, S. Assouline, Free flow at the interface of porous surfaces: a generalization of the Taylor brush configuration, Transport in Porous Media 54 (2004) 345–360.
[24] N.S. Abdullah, D.B. Das, H. Ye, Z.F. Cui, 3D bone tissue growth in hollow fibre membrane bioreactor: implications of various process parameters on tissue nutrition, The International Journal of Artificial Organs 29 (2006) 841–851.
[25] S. Shirazian, S.N. Ashrafizadeh, Mass transfer simulation of carbon dioxide absorption in a hollow-fiber membrane contactor, Separation Science and Technology 45 (2010) 515–524.
[26] H. Ye, D.B. Das, J.T. Triffitt, Z. Cui, Modelling nutrient transport in hollow fibre membrane bioreactors for growing three-dimensional bone tissue, Journal of Membrane Science 272 (2006) 169–178.
[27] N.S. Abdullah, D.B. Das, Modelling nutrient transport in hollow fibre membrane bioreactor for growing bone tissue with consideration of multi-component interactions, Chemical Engineering Science 62 (2007) 5821–5839.